Chapter 3
A Theoretical Framework for the Dynamics of Multiple Intrinsic Oscillators in Single Neurons

Michiel W.H. Remme, Máté Lengyel, and Boris S. Gutkin

Abstract The dendritic tree contributes significantly to the elementary computations a neuron performs while converting its synaptic inputs into action potential output. Traditionally, these computations have been characterized as both temporally and spatially localized. Under this account, neurons compute near-instantaneous mappings from their current input to their current output, brought about by somatic summation of dendritic contributions that are generated in functionally segregated compartments. However, recent evidence about the presence of oscillations in dendrites suggests a qualitatively different mode of operation: the instantaneous phase of such oscillations can depend on a long history of inputs, and, under appropriate conditions, even dendritic oscillators that are remote may interact through synchronization. Here, we develop a mathematical framework to analyze the interactions of local dendritic oscillations, and the way these interactions influence single cell computations. Combining weakly coupled oscillator methods with cable theoretic arguments, we derive phase-locking states for multiple oscillating dendritic compartments. We characterize how the phase-locking properties depend on key parameters of the oscillating dendrite: the electrotonic properties of the

M.W.H. Remme (✉)
Group for Neural Theory, Département d'Études Cognitives, École Normale Supérieure, Paris, France

Current address: Institute for Theoretical Biology, Humboldt-Universität zu Berlin, Berlin, Germany
e-mail: michiel.remme@hu-berlin.de

M. Lengyel
Computational and Biological Learning Lab, Department of Engineering, University of Cambridge, Cambridge, UK
e-mail: m.lengyel@eng.cam.ac.uk

B.S. Gutkin
Group for Neural Theory, Département d'Études Cognitives, École Normale Supérieure, Paris, France
e-mail: boris.gutkin@ens.fr

N.W. Schultheiss et al. (eds.), *Phase Response Curves in Neuroscience: Theory, Experiment, and Analysis*, Springer Series in Computational Neuroscience 6,
DOI 10.1007/978-1-4614-0739-3_3, © Springer Science+Business Media, LLC 2012

(active) dendritic segment, and the intrinsic properties of the dendritic oscillators. As a direct consequence, we show how input to the dendrites can modulate phase-locking behavior and hence global dendritic coherence. In turn, dendritic coherence is able to gate the integration and propagation of synaptic signals to the soma, ultimately leading to an effective control of somatic spike generation. Our results suggest that dendritic oscillations enable the dendritic tree to operate on more global temporal and spatial scales than previously thought; notably that local dendritic activity may be a mechanism for generating on-going whole-cell voltage oscillations.

1 Introduction

The dendritic tree contributes significantly to the elementary computations a neuron can perform, both by its intricate morphology and its composition of voltage-gated ionic conductances (Stuart et al. 2007). Such active conductances can underlie a wide variety of dynamical behaviors such as ongoing oscillations of the dendritic membrane potential, both sub- and supra-threshold. Membrane potential oscillations have been demonstrated in various types of neurons. Prominent intrinsic subthreshold oscillations have been found in stellate cells from entorhinal cortex layer 2 (Alonso and Llinás 1989; Alonso and Klink 1993), neurons from the frontal cortex (Gutfreund et al. 1995), neurons from the amygdala complex (Pape et al. 1998; Sanhueza and Bacigalupo 2005), and pyramidal cells and interneurons from the hippocampal CA1 area (Leung and Yim 1991; Chapman and Lacaille 1999).

Although these membrane potential oscillations are normally recorded at the soma and thus are considered to be of somatic origin, several lines of evidence suggest dendritic loci of generation. First, many of the conductances thought to underlie the generation of such oscillations reside predominantly in the dendrites, sometimes specifically in the distal parts of the dendritic tree. For example, in the apical dendrites of hippocampal CA1 pyramidal neurons, the density of I_h increases strongly with distance from the soma (Magee 1998), and reaches very high values in the thin distal branches (Lörincz et al. 2002). Second, several studies have suggested the existence of clusters of ionic conductances that are responsible for the generation of dendritic spikes (Llinás and Sugimori 1980). While most of the direct electrophysiological evidence regards excitable behavior, demonstrating the generation of dendritic spikes in response to sufficient levels of depolarization, mathematical analysis has shown that neural membranes exhibiting excitability can readily pass to oscillatory regimes in an input-dependent manner (e.g., see Rinzel and Ermentrout 1998). Third, in several cases, oscillations have been directly recorded in dendrites. For example, recordings from hippocampal CA1 pyramidal neurons have demonstrated ongoing oscillations in the dendrites that include repetitive dendritic spikes, presumably involving Ca^{2+} currents (Kamondi et al. 1998). Furthermore, significant intrinsic dendritic oscillations have been observed in several neuronal preparations that depended on the interplay between the nonlinear properties of NMDA synaptic receptors and intrinsic

voltage-dependent currents (Moore et al. 1999; Placantonakis and Welsh 2001). Crucially, while the onset of these oscillations was conditional on the activation of the NMDA synapses, the oscillations themselves were produced by mechanisms that were intrinsic to the postsynaptic cell and not by periodically structured synaptic inputs. Since NMDA receptors are largely localized on dendritic spines, and are hence electrotonically removed from the soma, these data may also argue for a nonuniform and local dendritic generation of membrane potential oscillations. Taken together, these experimental results suggest that dendritic trees can function as oscillators, perhaps conditional on the level of background depolarization or the presence of neuromodulators (Yoshida and Alonso 2007), while leaving open the question whether global cell-wide voltage oscillations could result from local dendritic mechanisms that are intrinsic even to distal dendrites and hence perhaps only weakly coupled to the soma electrotonically.

Indeed, multiple intrinsic dendritic oscillators have been proposed to underlie the recently discovered intricate firing pattern of entorhinal grid cells (O'Keefe and Burgess 2005; Burgess et al. 2007; Giocomo et al. 2007). This influential model suggests that the functional responses of entorhinal neurons recorded in behaving animals are a direct consequence of the generation of independent oscillations that are intrinsic to individual dendrites. Hence, this model presupposes the existence of multiple oscillators that are integrated at the soma, leading to the questions of how such dendritic oscillators may interact with the soma and with each other, and what sorts of collective behaviors the electrotonic structure of the dendritic tree might impose on the oscillations.

Here, we focus on the dynamics of such interacting oscillators and their impact on signal propagation in single neurons, using mathematical analysis corroborated by numerical simulations of biophysical models. We treat the dendritic tree of a neuron as a network of oscillators coupled by stretches of relatively less active cable. This prompts us to combine two analytical methods: weakly coupled oscillator theory and cable theory. The theory of weakly coupled oscillators has been extensively used previously to study synchronization of multiple oscillators residing in separate cells interacting through synapses or gap junctions (Izhikevich 2007). In this framework, the response of oscillators to perturbations is described by their infinitesimal phase response curves. This greatly simplifies this complex dynamical system and allows for an analytical treatment of the phase-locking behavior of the coupled oscillators. Since we focus on intradendritic oscillators, which are continuously coupled via the membrane voltage, we use cable theory (Rall 1967) to compute the perturbations via which the oscillators interact.

Part of the results of this chapter have been published in Remme et al. (2009).

2 Methods

We first develop a theory for the behavior of a dendritic tree that contains multiple intrinsic oscillators and then use this framework to gain understanding of how such a tree would behave dynamically and hence control the neuron's output depending on the input. In order to develop the mathematical framework, we begin by considering

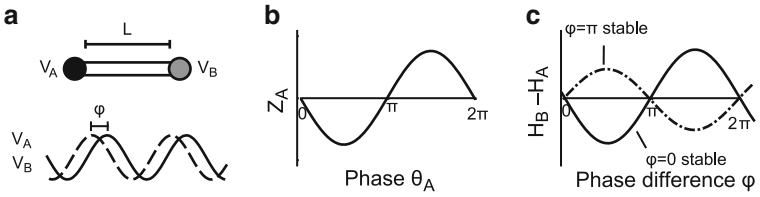

Fig. 3.1 Minimal system of two oscillators coupled via a dendritic cable. (**a**) The oscillators with voltage trajectories $V_A(t)$ and $V_B(t)$ and phase difference ϕ determine the membrane potential at the ends of a cable with electrotonic length L. (**b**) Example of a phase response function $Z_A(\theta_A)$ giving the phase shift of oscillator A as a perturbation at phase θ_A. (**c**) The stable phase-locked solution is determined by $\dot{\phi} = 0$ and $\frac{d}{d\phi}\dot{\phi} < 0$ and is either at $\phi = 0$ (e.g. for the *solid curve*) or at $\phi = \pi$ (e.g. for the *dash-dotted curve*)

a minimal setup of two cable-coupled oscillators. As we will see, even this setup is too complicated for direct analytical treatment; hence, we will go through a number of reduction steps which we sketch out below.

We study the behavior of a system of two oscillators with period T being connected via an active (though not intrinsically oscillating) dendritic cable with length constant λ and membrane time constant τ. The cable also expresses a voltage-dependent conductance with a gating variable $m(x,t)$ with activation function $m_\infty(V)$ and time constant τ_m (in milliseconds). The equations governing the membrane potential $V(x,t)$ and the gating variable $m(x,t)$ along the cable (excluding the oscillators) are

$$\begin{aligned}\tau\frac{\partial}{\partial t}V(x,t) &= \lambda^2\frac{\partial^2}{\partial x^2}V(x,t) - (V(x,t) - E_L) - \gamma_m\, m(x,t)\,(V(x,t) - E_m)\\ \tau_m\frac{\partial}{\partial t}m(x,t) &= m_\infty(V(x,t)) - m(x,t),\end{aligned} \tag{3.1}$$

where E_L is the leak reversal potential, E_m is the reversal potential of the active current, and γ_m is the ratio of the maximal conductance of the active current to the leak conductance. The two oscillators A and B are located at the ends of the cable at $x = 0$ and $x = l$, separated by an electrotonic distance $L = l/\lambda$ (Fig. 3.1a). The two oscillators form the periodically forced end conditions of the cable:

$$\begin{aligned}V(0,t) &= V_A(t),\\ V(l,t) &= V_B(t)\end{aligned} \tag{3.2}$$

with $V_A(t)$ and $V_B(t)$ being the voltage traces of the two oscillators A and B that evolve according to

$$\begin{aligned}C_m\frac{d}{dt}V_A(t) &= -g_L(V_A(t) - E_L) - I_A(V_A(t), \mathbf{m}_A(t)) - \varepsilon\, p_A(t),\\ C_m\frac{d}{dt}V_B(t) &= -g_L(V_B(t) - E_L) - I_B(V_B(t), \mathbf{m}_B(t)) - \varepsilon\, p_B(t),\end{aligned} \tag{3.3}$$

where C_m is the membrane capacitance (in $\mu F/cm^2$), g_L is the leak conductance (in mS/cm^2), $I_{A,B}(t)$ summarizes the voltage-dependent membrane currents generating the oscillations with the vector of gating variables $\mathbf{m}_{A,B}(t)$ given by standard kinetic equations. The terms $\varepsilon\, p_{A,B}(t)$ describe the perturbing currents that each oscillator receives from the cable and are proportional to $\frac{\partial}{\partial x}V(0,t)$ and $\frac{\partial}{\partial x}V(l,t)$. In the weak coupling framework ε is typically a small parameter, implying that the currents in the stretch of cell membrane that generate the intrinsic oscillations are much stronger than the perturbing currents that arrive from the dendritic cable, hence, $|\varepsilon\, p_{A,B}(t)|/|g_L(V_{A,B}(t) - E_L) + I_{A,B}(t)| \ll 1$. For a cable with diameter d (in cm) and oscillators that are described as a single isopotential compartment with membrane surface area A (in cm^2), we have $\varepsilon = \pi d^2/4R_i\, A$, where R_i is the intracellular resistivity of the dendritic cable (in $k\Omega$ cm).

The two oscillators described by (3.3) form the boundary conditions (3.2) for the cable (3.1). In turn, the cable yields the current flux through its ends into (and thereby perturbing) the two oscillators: the terms $\varepsilon\, p_{A,B}(t)$ in (3.3). It is clear that it is next to impossible to solve (3.1)–(3.3) directly. However, we will use a number of reductions to arrive at a phase description of the system that is simple enough to handle analytically. This allows us to derive interaction functions for the two oscillators, describing how much they perturb each other through the dendrite depending on their phases. We then use these interaction functions to determine the stable phase relationship between the oscillators for different parameters, i.e., the properties of the cable and the type of oscillators (see for similar approaches Crook et al. 1998; Bressloff 1999; Goldberg et al. 2006).

We begin by observing that the oscillators from (3.3) can be reduced to a phase description (Izhikevich 2007). The phases θ_A and θ_B (in radians) describe the state of each oscillator. The dynamics of the phases are then described by

$$\begin{aligned}\dot{\theta}_A &= \frac{2\pi}{T} + \varepsilon\, Z_A(t)\, p_A(t),\\ \dot{\theta}_B &= \frac{2\pi}{T} + \varepsilon\, Z_B(t)\, p_B(t).\end{aligned} \tag{3.4}$$

Here, the first term in the right hand side of each equation is the natural frequency of each oscillator and the second term describes the interaction between the oscillators. The crux of the analysis is thus to derive this function which we do explicitly in Appendix.

The interaction between the two oscillators depends on two factors: the intrinsic properties of the oscillators, as reflected by their infinitesimal phase response curves $Z_{A,B}(t)$, and the perturbations $p_{A,B}(t)$ to each oscillator via the cable. The infinitesimal phase response curve of an oscillator describes the phase shift induced by a perturbation delivered at a given phase (Fig. 3.1b). It can be determined using standard methods (Izhikevich 2007). The perturbations to the oscillators come from solving (3.1) with the oscillators described by (3.3) as the boundary conditions described by (3.2). For the active cable, this task can be greatly simplified if we consider a quasi-active approximation of the cable, and if we realize that the cable should behave periodically. The former can be done by linearizing the cable (3.1)

about the voltage to which the cable would relax if it was not driven by the oscillators (Sabah and Leibovic 1969; Koch 1984). Under such approximations, the active properties of the dendritic cable can be summarized by a single parameter, μ, which can be derived from its basic biophysical properties (see Appendix). The sign of μ indicates whether the active conductance that is present in the cable is regenerative ($\mu < 0$), restorative ($\mu > 0$), or passive ($\mu = 0$) (see also Goldberg et al. 2006). A regenerative current will amplify perturbations (e.g., a persistent sodium current I_{NaP}), while a restorative current actively counteracts such perturbations (e.g., the hyperpolarization activated inward current I_{h}).

Since the solution to the cable equation with periodically forced end conditions is also periodic, it depends only on the difference of the phases of the two oscillators $\phi = \theta_{\mathrm{B}}(t) - \theta_{\mathrm{A}}(t)$. The dynamics of ϕ is the central object of our interest. Assuming that the oscillator interactions via the cable are relatively weak, we can obtain the interaction functions $H_{\mathrm{A}}(\phi)$ and $H_{\mathrm{B}}(\phi)$ (see Izhikevich 2007 and Appendix). These describe the change in the oscillators' phases as a function of the phase difference (Fig. 3.1c). Now the phase difference between the oscillators evolves, on a slower timescale, as

$$\dot{\phi} = \varepsilon \left(H_{\mathrm{B}}(\phi) - H_{\mathrm{A}}(\phi) \right) \tag{3.5}$$

It is easy to see that phase-locked states for our dendrite can be identified as values of ϕ where $\dot{\phi} = 0$. The derivative of $\dot{\phi}$ with respect to ϕ gives the stability of such states (negative implies stable, positive unstable).

3 Results

3.1 Phase-Locking Dynamics of Specific Oscillator Models

The interaction functions and hence the phase-locking dynamics depend critically on the biophysics of the oscillators considered. We now turn to illustrating our analysis for two different oscillator types: one that generates action potentials and the other a model for subthreshold oscillations.

As a first example we analyze the phase-locking for the type II Morris–Lecar neural oscillator (Morris and Lecar 1981). The voltage trace and the phase response function of this oscillator are plotted in Fig. 3.2a for one oscillation cycle, starting at the peak of the voltage trace. With this, we can compute the bifurcation diagram and determine the stable and unstable phase-locked solutions as a function of the electrotonic distance L, one key parameter in determining the phase-locking dynamics (Fig. 3.2b). The dendrite shows a bistable region where both the in-phase and the antiphase solution are stable (around $L \sim 1.65$). For smaller L, the in-phase solution is stable. As the electrotonic separation between the oscillators approaches $L = 4$, there is also a sharp transition from a stable anti-phase to a stable in-phase solution.

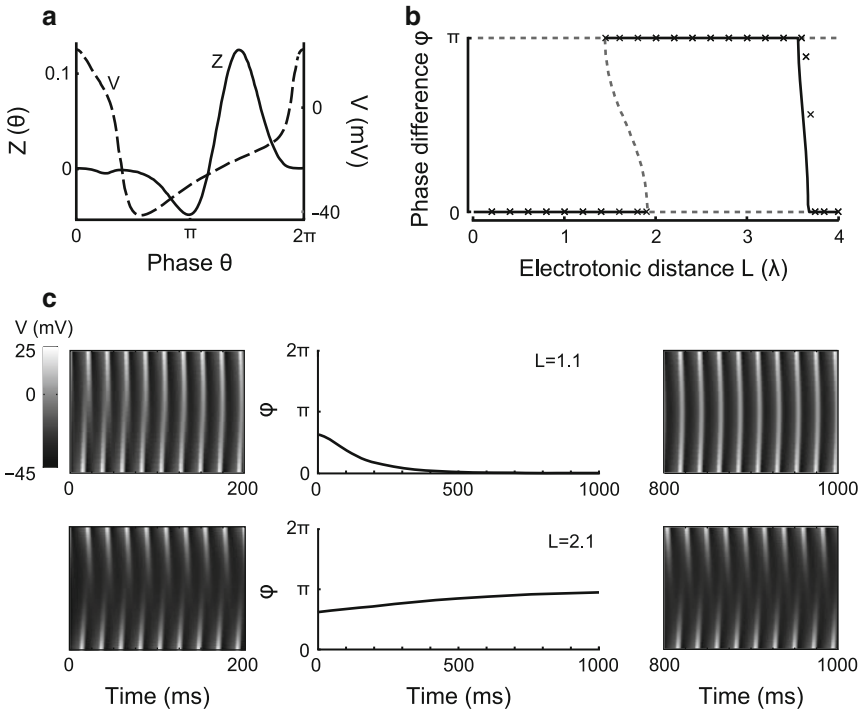

Fig. 3.2 Phase-locking of two Morris–Lecar type II oscillators. (**a**) Voltage trajectory (*dashed line*) and phase response function (*solid line*) of the Morris–Lecar type II oscillator with period $T = 21$ ms. (**b**) Bifurcation diagram showing the stable (*solid black line*) and unstable (*dashed gray line*) phase-locked solutions as a function of L. *Cross marks* give the stable phase difference determined with numerical simulations. (**c**) The *middle two panels* show simulations of the phase difference dynamics for $L = 1.1$ (*top*) and $L = 2.1$ (*bottom*). Space-time plots of the membrane potential along the dendritic cable are plotted for the first 200 ms (*left*) and for the final 200 ms (*right*) of the two simulations

Using numerical simulations of (3.1)–(3.3), we can demonstrate the dynamics of the phase difference between the two Morris–Lecar oscillators, as well as the membrane potential dynamics along the cable. Figure 3.2c illustrates these dynamics when the oscillators are separated by an electrotonic distance of $L = 1.1$ (top panels) or $L = 2.1$ (bottom panels). The oscillators start out with a phase difference of $\phi = 2\pi/3$. As expected from the bifurcation diagram in Fig. 3.2b, the two oscillators move to the in-phase configuration $\phi = 0$ when $L = 1.1$, synchronizing the voltage oscillations along the cable. When $L = 2.1$ the two oscillators settle in the antiphase solution $\phi = \pi$, producing large voltage gradients along the cable.

As a second example, we determine the phase locking for a model of subthreshold oscillations in entorhinal stellate cells under both passive and active cable coupling. These oscillations are thought to arise from an interaction between a

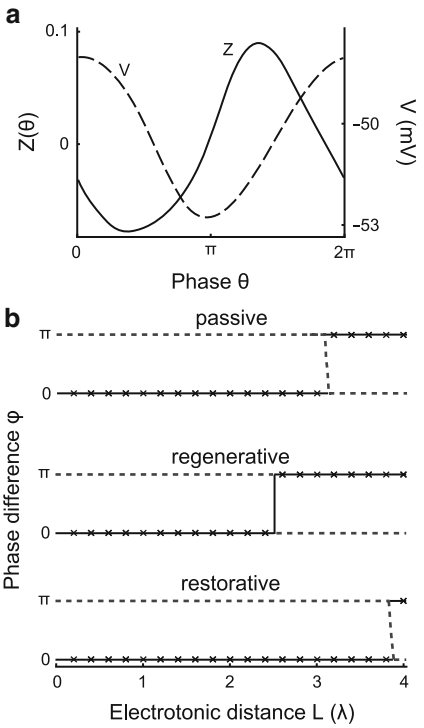

Fig. 3.3 Phase locking behavior of subthreshold oscillators. The oscillations are generated by interactions between I_{NaP} and I_{h} (see Appendix). (**a**) Voltage trajectory (*solid line*) and phase response function (*dashed line*) of the oscillator. (**b**) Bifurcation diagrams showing the stable (*solid black lines*) and unstable (*dashed gray lines*) phase-locked solutions as a function of L for a passive cable (*top*), a cable with a regenerative current (*middle*), and a cable with a restorative current (*bottom*). The restorative current I_{h} and regenerative current I_{NaP} are inserted in the cable using, respectively, $\mu = -1.35$, $\gamma_{\mathrm{R}} = 1.1$ and $\tau_{\mathrm{m}} = 1$ ms, and $\mu = 0.84$, $\gamma_{\mathrm{R}} = 1.21$ and $\tau_{\mathrm{m}} = 52.3$ ms. *Cross marks* in the bifurcation diagrams give the stable phase difference determined with numerical simulations of the nonlinear system

persistent sodium current I_{NaP} and a hyperpolarization-activated inward current I_{h} (see Appendix). Both the voltage trajectory and the phase response function are close to a sinusoid (Fig. 3.3a). The bifurcation diagrams (Fig. 3.3b) are shown for two oscillators coupled via a passive cable (top), a cable with a regenerative current (middle), and a cable with a restorative current (bottom). The regenerative current makes the transition between in-phase and antiphase solutions to occur for smaller L, compared to passive cable coupling. In contrast, adding the restorative current to the cable causes the transition to occur at larger L, making the synchronous phase-locked solution stable up to $L \sim 3.8$.

Numerical simulations of (3.1)–(3.3) agree very well with the theoretical predictions of the phase-locking, both for the type II Morris-Lecar oscillators (Fig. 3.2) and the subthreshold oscillators (Fig. 3.3), when using the maximal ε that still allows for oscillations. Larger values of ε lead to such strong interaction currents that

the oscillations are annihilated. Numerical simulations of (3.1)–(3.3) using voltage-dependent cable currents match exactly with the predictions of the weak coupling analysis (bottom two panels in Fig. 3.3b), thereby also emphasizing the validity of using linearized descriptions of those active currents in our analytical framework.

3.2 Multiple Oscillators: Chains and Branched Structures

So far, we have focused on a minimal configuration of two oscillators connected by a cable. However, our analysis can be easily extended to predict phase locking of a chain of oscillators. This follows since the phase-locking behavior only depends on each neighboring pair of oscillators. Figure 3.4a shows numerical simulations of a chain of three oscillators, using the same Morris–Lecar model as in Fig. 3.2. The two pairs are separated by a passive dendritic cable of either $L = 1.1$ (top panel) or $L = 2.1$ (bottom panel). The phase-locked solutions follow from the bifurcation diagram in Fig. 3.2b: the three oscillators move into an in-phase solution for $L = 1.1$, whereas for $L = 2.1$ each neighboring pair of oscillators moves into the anti-phase solution.

Our framework also allows us to understand phase locking in a branched cable structure. Hence, we examined the phase difference dynamics of a triangular configuration of three Morris–Lecar oscillators (Fig. 3.4b). In this situation, each oscillator is separated from the other two oscillators by a passive dendritic cable with electrotonic length $L = 1.1$ (top panel) or $L = 2.1$ (bottom panel). For $L = 1.1$, all three oscillators synchronize. When $L = 2.1$, we expect from the bifurcation diagram in Fig. 3.2c that the oscillators go into antiphase. However, as we have three mutually coupled oscillators, two pairs of antiphase locked oscillators would lead to an in-phase configuration of the final pair of oscillators. The bifurcation diagram shows that the in-phase configuration is unstable. We see from the simulation that the system settles into the solution closest to the antiphase solution, which is a phase difference of $2\pi/3$ between each pair of oscillators.

3.3 Dendritic Phase-Locked States: Controlled by Inputs and Read Out with Spikes

Above, we developed a framework for analyzing the behavior of local oscillators embedded in the dendritic tree. Now we turn to the question of how such oscillating dendrites respond to inputs and impact the output of the neuron. We will show that the external synaptic input can control the phase-locked configuration of the dendritic oscillators and that this phase-locked configuration can then be transmitted through patterning of the cell's action potentials. We give several salient illustrative examples using a model with a branched oscillating dendritic tree and a spike-generating soma. The model consists of a passive branching dendritic compartment

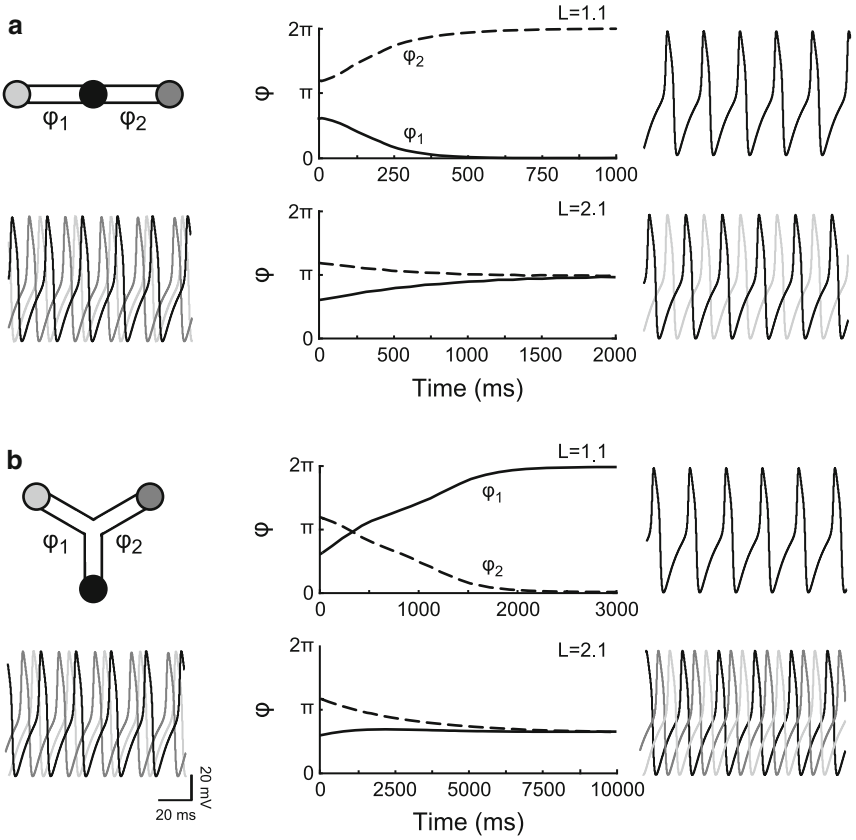

Fig. 3.4 Phase difference dynamics of three oscillators in a chain or a branched configuration. The Morris-Lecar type II oscillators are separated by a passive cable. Panels (**a**) and (**b**) show from *left to right*: a scheme of the model with below it the membrane potential of the oscillators at the start of the simulation; the dynamics of the phase difference ϕ between the oscillators for $L = 1.1$ (*top*) and $L = 2.1$ (*bottom*); and the membrane potential of the oscillators at the end of the simulation. The properties of the Morris-Lecar oscillators and the dendritic cable are as in Fig. 3.2

with two Morris–Lecar type II oscillators at its two distal ends and an excitable soma that, for simplicity, we describe with an integrate and fire mechanism (Fig. 3.5a).

Above, we showed that the dendritic tree can be in a phase-locking regime where two stable phase-locked states coexist (see Fig. 3.2b). In such a bistable regime, well-timed inputs to one or more dendritic oscillators can switch the locking between in-phase and anti-phase. Clearly, the membrane potential fluctuations at the soma depend on whether the dendritic oscillators are synchronized or not. In our model, they are largest in amplitude when the dendritic oscillators are in-phase. The soma can show this difference with its spiking pattern when such large amplitude fluctuations are supra-threshold, while smaller fluctuations (e.g., with asynchronous oscillators) are not.

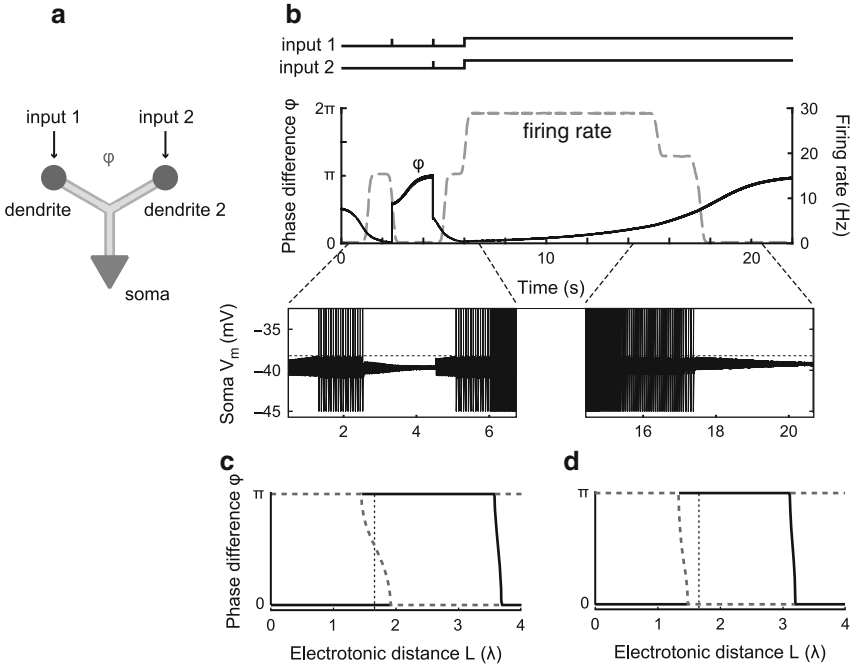

Fig. 3.5 Changing the phase-locked solution of dendritic oscillators with external input and detection of the phase-locked state with an excitable soma. (**a**) Schematic drawing showing the configuration of two dendritic Morris-Lecar type II oscillators and a spike-generating soma. All are separated by a passive cable with electrotonic length $L = 1.65$ and $\tau = 20$ ms. (**b**) From *top to bottom* are shown the inputs to the two dendritic oscillators, the phase difference dynamics (*solid black line*) and somatic firing rate (*dashed gray line*), and the somatic membrane potential V_m (*solid line*) with the spike threshold (*dotted line*). Note that the spikes have been cut off in order to show the subthreshold membrane potential. (**c**–**d**) Bifurcation diagrams describing the phase-locked solutions up to $t = 6$ s (C, see also Fig. 3.2b) and after $t = 6$ s (D) with *dotted line* at $L = 1.65$ giving the electrotonic distance between the dendritic oscillators

In Fig. 3.5, we illustrate the above mechanism. The initial parameters are such that both the in-phase and antiphase state of the dendritic oscillators are stable (vertical dotted line in Fig. 3.5c). Oscillators starting from an initial phase difference $\phi = \pi/4$ move into the synchronous phase-locked state (solid black line in Fig. 3.5b, top panel). This consequently leads to repetitive somatic spiking (Fig. 3.5b, top panel shows firing rate and bottom panel shows zooms of somatic voltage). A brief depolarizing current pulse to one of the oscillators moves them into the antisynchronous state and the somatic spiking ceases. A subsequent synchronous current pulse to both dendritic oscillators can switch them back into the synchronous state and hence restart the spiking. Note that all the stimuli here are excitatory, yet depending on their timing, they can have a net excitatory or inhibitory effects on the cell's spiking.

Another mechanism by which inputs to the dendrites can affect the phase-locked state is by changing the input amplitude and thereby the oscillator frequency. In Fig. 3.5b at time $t = 6$ s we increase the amplitude of the current input impinging on the oscillators which causes the system to move out of the bistable regime. The synchronized state loses stability and the oscillators gradually move into anti-phase locking. As a result, the soma stops spiking (at time $t \sim 17$ s). Note that the electrotonic separation between the oscillators remains constant (vertical dotted line in Fig. 3.5d) but that the bifurcation diagram itself changes. In turn, a decrease in the excitatory input would reinstate spiking. Hence, this mechanism allows the cell to encode an inverse of the input amplitude, or the inverse of the excitatory input rate.

4 Discussion

We studied the dynamics of dendrites that show intrinsic oscillations due to active voltage-dependent currents that present strong spatial inhomogeneities, hence leading to discrete oscillatory segments. We developed an analytical framework to describe and understand the behavior of interacting dendritic oscillators and their impact on signal propagation within a neuron. A major focus was to understand when the oscillators within the dendrite would lock and hence the whole dendritic tree would act as a single oscillatory unit.

Using the weakly coupled oscillator framework, we have identified the requirements for the various phase-locking regimes of the dendritic oscillators. A central parameter determining the phase-locked solutions is the electrotonic distance between the oscillators. This distance determines how strongly the dendritic cable filters the interactions between the oscillators. In particular, dendritic coupling introduces a delay in the oscillator interactions. The time it takes for the state of one oscillator to perturb another oscillator increase with electrotonic distance, and thereby effectively shifts the phase response function (see also Goldberg et al. 2006). For tightly coupled oscillators, the synchronous solution is stable, and the antiphase solution is unstable. However, at a certain electrotonic distance, the phase response functions of the oscillators are shifted in time such that the synchronous solution loses stability and the antiphase solution becomes stable. Hence, the phase locking of oscillators alternates between synchronized solutions and anti-phase solutions as a function of the electrotonic distance.

The analysis also reveals how the phase-locking is affected by the presence of voltage-dependent conductances in the cable connecting the oscillators. Using the quasi-active approximation of the cable (Sabah and Leibovic 1969; Koch 1984), we find that the dependence of the stable phase-locked solution on the electrotonic distance is amplified by regenerative conductances (i.e., ionic conductances that amplify a voltage perturbation), whereas it is counteracted by restorative conductances (i.e., ionic conductances that counteract voltage perturbations) (see also Goldberg et al. 2006). It should be noted that the linearization of the active conductances in the dendrites is appropriate for small amplitude oscillations in the dendrite and is

therefore in general a better approximation for subthreshold oscillations than for spiking oscillators. The effects of active conductances in the connecting cable are explored in more detail in Remme et al. (2009), where we show that the above results hold in general.

The mathematical approach that we used, builds on several studies which focused on the interaction between two neurons with repetitively spiking somata that interact via inputs at the dendrites (Crook et al. 1998; Bressloff 1999; Goldberg et al. 2006). A crucial difference with these studies is that rather than coupling via discrete synaptic events, we treat continuous coupling between the oscillators via the current-conducting cables. One consequence of the continuous coupling is that one needs both the phase response function and the voltage trajectory of the oscillators in order to compute the interaction functions and ultimately the phase-locked solutions. Both the voltage trajectory of an oscillator and its phase response function can be determined numerically from a model of an oscillator and, at least in principle, also experimentally (see, e.g., Galán et al. 2005).

In the final section of our study, we demonstrated how inputs to the dendritic tree can set the phase-locked state and how in turn the phase-locked configuration can control somatic spike generation. The first can for instance be accomplished by changing the frequency of the oscillators with the external input. The soma can subsequently detect the amplitude of the membrane potential fluctuations since this is affected by the phase-locked configuration. The time scale at which the dendritic oscillators move from one solution to another is set by the strength of the interactions between the oscillators. This time scale can be much longer than that of the different components of the system, e.g., the membrane time constant or the period of the oscillators. In this way, the phase difference between the oscillators can function as a memory. Related ideas have been previously discussed by Huhn et al. (2005). We also showed that in the bistable phase-locked regime the state of the dendrites is easily set by transient inputs and "read-out" by the soma. This also can endow the neuron with a memory since brief external inputs can switch the neuron from a spiking to a quiescent mode and vice versa. Interestingly, we showed that both the turn-on and turn-off signals (inputs) can be excitatory, their final effects defined by their timing.

The focus of our report is complementary to that of a recent theoretical study of the subthreshold oscillations in the dendrites of mesencephalic dopaminergic neurons (Medvedev et al. 2003). As these cells do not show any indication of distinct dendritic oscillators, the whole cell was modeled as one continuous oscillator with gradients in oscillator properties along the dendrites. Moreover, since there were no distinct oscillators, in their analysis Medvedev and colleagues assumed strong voltage coupling between neighboring compartments, enforcing synchronized oscillations throughout the cell. In contrast, our approach assumed weak coupling between the dendritic oscillators. This would not be appropriate for a spatially continuous oscillator. However, it is not possible to state in general at what precise electrotonic distance between two oscillators the weak coupling assumption becomes valid, since it depends on the strength of the interaction currents with respect to the intrinsic currents of the oscillators. However, our numerical simulations for a dendritic

cable without the assumption of weak coupling, show that the phase-locking behavior of Morris-Lecar oscillators is consistent with weak coupling.

We have set up an analytical framework for studying interacting dendritic oscillators. This opens up a wide range of questions that were outside the scope of the present study. For example, we focused our analysis on identical oscillators, while it is likely that dendritic oscillators will vary in their properties throughout the dendritic tree. For example, the diameter of the dendrites, which typically becomes smaller with increasing distance from the soma, can affect the intrinsic frequency of the oscillators. A gradient in the frequency of distinct oscillators is likely to lead to more complex phenomena such as traveling waves (see, e.g., Kopell and Ermentrout 1986).

A major focus of our study was to explore how local dendritic mechanisms may lead to oscillations expressed globally in the cell and hence visible at the soma, for example, in somatic intracellular recordings. Our analysis showed that even electrotonically far removed dendritic oscillators can lead to voltage oscillations that significantly affect the soma voltage and hence spike generation. This suggests several experimentally testable predictions. In one possible experiment, one can take advantage of imperfect space clamp in a electrotonically extended neuron. As a proof of principle, in a neuron where the oscillations are generated distally in the dendritic tree, voltage clamping the soma would not block such oscillations, and these should be seen in the current necessary to hold the somatic potential. In fact, results from (Moore et al. 1999) point in this direction, where in chick spinal cord neuron NMDA-dependent intrinsic oscillations were not blocked by somatic voltage clamp. A further prediction stems from the weak coupling between active dendrites. If active oscillations, such as periodically generated dendritic spikes, are generated in different segments of the dendritic tree, our analysis predicts that such spikes should interact and should exist in a stable phase-locked configuration, e.g., synchrony. Hence, should one of the dendritic segments be phase-shifted, such perturbation should propagate to the other segment (the other segment should be phase reset), the dendritic spikes should return to the phase-locked configuration, and the time scale of this return should be relatively long and determined by the electrotonic distance between the active segments. While difficult, such experiments are possible using the multiple dendritic recording techniques, such as those developed by Davie et al. (2006) in Purkinje cells.

A recent model for the grid field properties of the entorhinal cortex layer II stellate cells (O'Keefe and Burgess 2005; Burgess et al. 2007; Hasselmo 2007) relies precisely on the ingredients considered in the present study. The model assumes that different dendritic branches emanating from the soma of these cells function as distinct oscillators. The oscillations are modulated by external inputs and the interference of the oscillators eventually determines the somatic spiking. Crucially, the model assumes that the dendritic oscillators operate independently. At a first glance, our results appear to argue against this: the various oscillators should phase lock (hence, lose their independence) even when the mutual coupling is weak. However, in principle, the locking may be slower than the behavioral time scale, allowing the oscillators to act quasi-independently on the behavioral time scale.

Our analysis provides the appropriate framework to examine these issues: the scaling of locking in time and the biophysical implementation of grid-field formation via dendritic oscillators (see Remme et al. 2010).

Above, we studied relatively simple cell geometries; however, these form basic building blocks for more complex dendritic trees. Thus our framework should be valid for understanding global voltage oscillations in more realistic models of spatially extended cells. We would like to emphasize at this point that our general framework should also hold when – in addition to the distinct oscillators distributed throughout the dendritic tree – also the soma is regarded as an oscillator. These and other issues will be addressed in future publications.

The framework we have developed, builds on the extensive mathematical theory of coupled oscillators and nestles nicely below the complexity of full compartmental models of neuronal dendritic trees. Yet our framework is sufficiently powerful and clear to both take into account certain key aspects of the dendritic tree structure and to be amenable to theoretical analysis of the dynamics of active dendrites and the computational function of such dendritic structures. These remain an active focus for further investigations.

Appendix

Interaction Functions for Two Weakly Coupled Dendritic Oscillators

In order to determine the perturbations $\varepsilon\, p_{\mathrm{A,B}}(t)$ in (3.3), we need to solve (3.1) with the boundary conditions from (3.2). To do so, we linearize (3.1) about the membrane potential V_{R} to which the cable would relax if it was not driven by the oscillators, yielding the quasi-active approximation for the cable (Sabah and Leibovic 1969; Koch 1984). This approximation is appropriate as long as the voltage fluctuations around V_{R} are sufficiently small. We define $U(x,t)$ as the difference between the oscillating solution and the resting membrane potential V_{R}, i.e., $U(x,t) \equiv V(x,t) - V_{\mathrm{R}}$ and we define $w(x,t)$ analogously as $w(x,t) \equiv m(x,t) - m_\infty(V_{\mathrm{R}})$. The equations describing the quasi-active cable now read

$$\begin{aligned} \tau \frac{\partial}{\partial t} U(x,t) &= \lambda^2 \frac{\partial^2}{\partial x^2} U(x,t) - \gamma_{\mathrm{R}}\, U(x,t) - \gamma_{\mathrm{m}}(V_{\mathrm{R}} - E_{\mathrm{m}})\, w(x,t) \\ \tau_{\mathrm{m}} \frac{\partial}{\partial t} w(x,t) &= \frac{\partial}{\partial V} m_\infty(V_{\mathrm{R}})\, U(x,t) - w(x,t), \end{aligned} \tag{3.6}$$

where $\gamma_{\mathrm{R}} = 1 + \gamma_{\mathrm{m}} m_\infty(V_{\mathrm{R}})$ is the total membrane conductance of the cable at V_{R} divided by the cable's membrane leak conductance.

The oscillators determine the voltage of the cable at $x = 0$ and $x = l$. These voltages would need to be computed by solving the full system of equations for the dynamics of each oscillator; however, since we consider weak coupling (meaning that the trajectories are only weakly perturbed by the cable currents) we

can make use of the fact that the trajectories are periodic. Hence, we expand U_A and U_B in a Fourier series, allowing for a possible phase difference ϕ (in radians) between the oscillators:

$$\begin{aligned} U(0,t) &= U_\mathrm{A}(t) = \sum_{n=-\infty}^{\infty} \widetilde{U}_n^\mathrm{A}\, \mathrm{e}^{\mathrm{i}\omega_n t}, \\ U(l,t) &= U_\mathrm{B}\left(t + \phi\tfrac{T}{2\pi}\right) = \sum_{n=-\infty}^{\infty} \widetilde{U}_n^\mathrm{B}\, \mathrm{e}^{\mathrm{i}(\omega_n t + n\phi)}, \end{aligned} \tag{3.7}$$

where $\omega_n = n\,2\pi/T$, T is the intrinsic oscillator period, and membrane voltages U_A and U_B (in mV) are measured relative to V_R.

The solution of the cable (3.6) will also be periodic and we can write the equation in the frequency domain as

$$\lambda^2 \frac{d^2}{dx^2}\widetilde{U}_n(x) - \left(\gamma_\mathrm{R} + \frac{\mu}{1+(\omega_n\tau_\mathrm{m})^2} + i\,\omega_n\left(\tau - \frac{\mu\,\tau_\mathrm{m}}{1+(\omega_n\tau_\mathrm{m})^2}\right)\right)\widetilde{U}_n(x) = 0. \tag{3.8}$$

Using the boundary conditions defined by (3.7) yields the solution:

$$U(x,t) = \sum_{n=-\infty}^{\infty} \mathrm{e}^{\mathrm{i}\omega_n t}\,\widetilde{U}_n^\mathrm{A}\frac{\sinh\left(b_n(L-x/\lambda)\right)}{\sinh\left(b_n\,L\right)} + \sum_{n=-\infty}^{\infty} \mathrm{e}^{\mathrm{i}(\omega_n t+n\phi)}\,\widetilde{U}_n^\mathrm{B}\frac{\sinh\left(b_n\,x/\lambda\right)}{\sinh\left(b_n\,L\right)}, \tag{3.9}$$

where

$$b_n = \sqrt{\gamma_\mathrm{R} + \frac{\mu}{1+(\omega_n\tau_\mathrm{m})^2} + i\,\omega_n\left(\tau - \frac{\mu\,\tau_\mathrm{m}}{1+(\omega_n\tau_\mathrm{m})^2}\right)} \tag{3.10}$$

with $\mu = \gamma_\mathrm{m}(V_\mathrm{R}-E_\mathrm{m})\frac{\partial}{\partial V}m_\infty(V_\mathrm{R})$. The parameter μ determines whether the active conductance that is present in the cable is regenerative ($\mu < 0$), meaning that perturbations are amplified (e.g., a persistent sodium current), or restorative ($\mu > 0$), meaning that the active conductance counteracts perturbations from V_R (e.g., the hyperpolarization activated inward current). As mentioned above, the perturbations that the oscillators receive from the cable is proportional to the derivative of the voltage with respect to x. For the oscillator at $x = 0$, the perturbation from the cable is

$$\begin{aligned} p_\mathrm{A}(t;\phi) &= \frac{\partial}{\partial x}U(0,t) \\ &= \frac{1}{\lambda}\sum_{n=-\infty}^{\infty} \mathrm{e}^{\mathrm{i}(\omega_n t+n\phi)}\,\widetilde{U}_n^\mathrm{B}\,\frac{b_n}{\sinh\left(b_n\,L\right)} - \frac{1}{\lambda}\sum_{n=-\infty}^{\infty} \mathrm{e}^{\mathrm{i}\omega_n t}\,\widetilde{U}_n^\mathrm{A}\,b_n\coth\left(b_n\,L\right) \\ &= \frac{1}{\lambda}\sum_{n=-\infty}^{\infty} \mathrm{e}^{\mathrm{i}\omega_n t}\,\frac{b_n}{\sinh(b_n\,L)}\left(\widetilde{U}_n^\mathrm{B}\,\mathrm{e}^{\mathrm{i}n\phi} - \widetilde{U}_n^\mathrm{A}\,\cosh(b_n\,L)\right). \end{aligned} \tag{3.11}$$

The perturbation from the cable at $x = l$ can be derived in the same way.

We have now derived the perturbations that an oscillator receives depending on the phase difference ϕ between the oscillators. In order to complete our analysis, we also need to compute how these perturbations act back on the phases of the two oscillators and thus on the phase difference. Each of the oscillators is described explicitly by a system of equations determining the dynamics of its voltage (3.3). However, if we assume that the periodic solutions of such a system of equations are sufficiently attractive and the coupling is sufficiently weak we can write an equivalent phase model (see Izhikevich 2007). The phases of the two dendritic oscillators, $\theta_{\mathrm{A}}(t)$ and $\theta_{\mathrm{B}}(t)$ (in radians), evolve as

$$\begin{aligned}\dot{\theta}_{\mathrm{A}} &= \frac{2\pi}{T} + \varepsilon\, Z_{\mathrm{A}}(\theta_{\mathrm{A}})\, p_{\mathrm{A}}\left(\theta\frac{T}{2\pi};\phi\right),\\ \dot{\theta}_{\mathrm{B}} &= \frac{2\pi}{T} + \varepsilon\, Z_{\mathrm{B}}(\theta_{\mathrm{B}})\, p_{\mathrm{B}}\left(\theta\frac{T}{2\pi};\phi\right),\end{aligned} \tag{3.12}$$

where $\frac{2\pi}{T}$ is the intrinsic oscillator frequency. The second term describes the effect of the cable on the phase. $Z_{\mathrm{A,B}}(\theta)$ are the infinitesimal phase response functions of the respective oscillators and describe how much their phases are advanced or delayed in response to an infinitesimally small and short perturbation.

Since we consider weak interactions between the oscillators, ϕ changes slowly with respect to the oscillation period. Therefore, we can average the interaction between the oscillators (i.e., the products $Z_{\mathrm{A}}\, p_{\mathrm{A}}$ and $Z_{\mathrm{B}}\, p_{\mathrm{B}}$ in (3.12)) over a cycle and obtain the interaction functions $H_{\mathrm{A,B}}(\phi)$. $H_{\mathrm{A}}(\phi)$ describes the average effect on the phase of oscillator A over one cycle as a function of ϕ:

$$H_{\mathrm{A}}(\phi) = \frac{1}{2\pi}\int_0^{2\pi} Z_{\mathrm{A}}(\theta)\, p_{\mathrm{A}}\left(\theta\frac{T}{2\pi};\phi\right)\, d\theta \tag{3.13}$$

with p_{A} given by (3.11). The interaction function $H_{\mathrm{B}}(\phi)$ can be determined analogously. Note that with identical oscillators, we have $H_{\mathrm{B}}(\phi) = H_{\mathrm{A}}(-\phi)$.

Oscillator Models

The equations for the Morris–Lecar type II oscillator (Morris and Lecar 1981) with parameters as in Ermentrout (1996) read

$$\begin{aligned}C_{\mathrm{m}}\frac{\mathrm{d}V}{\mathrm{d}t} &= -g_{\mathrm{L}}(V-E_{\mathrm{L}}) - g_{\mathrm{w}}\, w(V-E_{\mathrm{w}}) - g_{\mathrm{m}}\, m_{\infty}(V)(V-E_{\mathrm{m}}) + I\\ \frac{\mathrm{d}w}{\mathrm{d}t} &= \varphi\frac{w_{\infty}(V)-w}{\tau_{\mathrm{w}}(V)}.\end{aligned} \tag{3.14}$$

The Morris–Lecar type II oscillator uses $C_m = 1\,\mu F/cm^2$, $g_L = 0.5\,mS/cm^2$, $g_w = 2\,mS/cm^2$, $g_m = 1.1\,mS/cm^2$, $E_L = -50\,mV$, $E_w = -70\,mV$, $E_m = 100\,mV$, $\varphi = 0.2$, $I = 25\,\mu A/cm^2$, and where $m_\infty(V) = \frac{1}{2}[1 + \tanh((V + 1)/15)]$, $w_\infty(V) = \frac{1}{2}[1 + \tanh(V/30)]$, and $\tau_w(V) = 1/\cosh(V/60)$.

The oscillatory dynamics of the subthreshold oscillator emerge from the interaction between the persistent sodium current I_{NaP} and the hyperpolarization activated inward current I_h. The current descriptions are based on the data from Dickson et al. (2000) and Fransén et al. (2004). The dynamics of I_h are described by a single gating variable $w(t)$ with activation function $w_\infty(V)$ and time constant $\tau_w(V)/\varphi$ (in milliseconds). The voltage-dependent activation of I_{NaP} is described by $m_\infty(V)$ and is instantaneous. The equations are the same as for the Morris–Lecar type II oscillator with $C_m = 1\,\mu F/cm^2$, $g_L = 0.3\,mS/cm^2$, $g_w = 1.5\,mS/cm^2$, $g_m = 0.076\,mS/cm^2$, $E_L = -69\,mV$, $E_w = -20\,mV$, $E_m = 48\,mV$, $\varphi = 0.014$, $I = 0.9\,\mu A/cm^2$, and where $m_\infty(V) = \frac{1}{2}[1 + \tanh((V + 48.7)/8.8)]$, $w_\infty(V) = \frac{1}{2}[1 + \tanh((V + 74.2)/-14.4)]$, and $\tau_w(V) = 1/\cosh((V + 74.2)/-28.8)$.

References

Alonso, A. and Klink, R. (1993). Differential electroresponsiveness of stellate and pyramidal-like cells of medial entorhinal cortex layer II. *J Neurophysiol*, 70(1):128–43.

Alonso, A. and Llinás, R. (1989). Subthreshold Na^+-dependent theta-like rhythmicity in stellate cells of entorhinal cortex layer II. *Nature*, 342(6246):175–7.

Bressloff, P. C. (1999). Resonantlike synchronization and bursting in a model of pulse-coupled neurons with active dendrites. *J Comput Neurosci*, 6(3):237–49.

Burgess, N., Barry, C., and O'Keefe, J. (2007). An oscillatory interference model of grid cell firing. *Hippocampus*, 17(9):801–12.

Chapman, C. A. and Lacaille, J. C. (1999). Intrinsic theta-frequency membrane potential oscillations in hippocampal CA1 interneurons of stratum lacunosum-moleculare. *J Neurophysiol*, 81(3):1296–307.

Crook, S., Ermentrout, G., and Bower, J. (1998). Dendritic and synaptic effects in systems of coupled cortical oscillators. *J Comput Neurosci*, 5(3):315–29.

Davie, J. T., Kole, M. H. P., Letzkus, J. J., Rancz, E. A., Spruston, N., Stuart, G. J., and Häusser, M. (2006). Dendritic patch-clamp recording. *Nat Protoc*, 1(3):1235–47.

Dickson, C., Magistretti, J., Shalinsky, M., Fransén, E., Hasselmo, M., and Alonso, A. (2000). Properties and role of I_h in the pacing of subthreshold oscillations in entorhinal cortex layer II neurons. *J Neurophysiol*, 83(5):2562–79.

Ermentrout, G. B. (1996). Type I membranes, phase resetting curves, and synchrony. *Neural Comp*, 8(5):979–1001.

Fransén, E., Alonso, A., Dickson, C. T., Magistretti, J., and Hasselmo, M. E. (2004). Ionic mechanisms in the generation of subthreshold oscillations and action potential clustering in entorhinal layer II stellate neurons. *Hippocampus*, 14(3):368–84.

Galán, R. F., Ermentrout, G. B., and Urban, N. N. (2005). Efficient estimation of phase-resetting curves in real neurons and its significance for neural-network modeling. *Phys Rev Lett*, 94(15):158101.

Giocomo, L., Zilli, E., Fransén, E., and Hasselmo, M. (2007). Temporal frequency of subthreshold oscillations scales with entorhinal grid cell field spacing. *Science*, 315(5819):1719–22.

Goldberg, J., Deister, C., and Wilson, C. (2006). Response properties and synchronization of rhythmically firing dendritic neurons. *J Neurophysiol*, 97(1):208–19.

Gutfreund, Y., Yarom, Y., and Segev, I. (1995). Subthreshold oscillations and resonant frequency in guinea-pig cortical neurons: physiology and modelling. *J Physiol*, 483 (Pt 3):621–40.

Hasselmo, M. E. (2007). Arc length coding by interference of theta frequency oscillations may underlie context-dependent hippocampal unit data and episodic memory function. *Learn Mem*, 14(11):782–94.

Huhn, Z., Orbán, G., Érdi, P., and Lengyel, M. (2005). Theta oscillation-coupled dendritic spiking integrates inputs on a long time scale. *Hippocampus*, 15(7):950–62.

Izhikevich, E. (2007). *Dynamical Systems in Neuroscience: The Geometry of Excitability And Bursting*. Cambridge, MA: MIT Press.

Kamondi, A., Acsády, L., Wang, X.-J., and Buzsáki, G. (1998). Theta oscillations in somata and dendrites of hippocampal pyramidal cells *in vivo*: activity-dependent phase-precession of action potentials. *Hippocampus*, 8(3):244–61.

Koch, C. (1984). Cable theory in neurons with active, linearized membranes. *Biol Cyber*, 50(1): 15–33.

Kopell, N. and Ermentrout, G. B. (1986). Symmetry and phaselocking in chains of weakly coupled oscillators. *Comm Pure Appl Math*, 39(5):623–660.

Leung, L. W. and Yim, C. Y. (1991). Intrinsic membrane potential oscillations in hippocampal neurons *in vitro*. *Brain Res*, 553(2):261–74.

Llinás, R. R. and Sugimori, M. (1980). Electrophysiological properties of *in vitro* Purkinje cell dendrites in mammalian cerebellar slices. *J Physiol*, 305:197–213.

Lörincz, A., Notomi, T., Tamás, G., Shigemoto, R., and Nusser, Z. (2002). Polarized and compartment-dependent distribution of HCN1 in pyramidal cell dendrites. *Nat Neurosci*, 5(11):1185–93.

Magee, J. C. (1998). Dendritic hyperpolarization-activated currents modify the integrative properties of hippocampal CA1 pyramidal neurons. *J Neurosci*, 18(19):7613–24.

Medvedev, G. S., Wilson, C. J., Callaway, J. C., and Kopell, N. J. (2003). Dendritic synchrony and transient dynamics in a coupled oscillator model of the dopaminergic neuron. *J Comput Neurosci*, 15(1):53–69.

Moore, L. E., Chub, N., Tabak, J., and O'Donovan, M. (1999). NMDA-induced dendritic oscillations during a soma voltage clamp of chick spinal neurons. *J Neurosci*, 19(19):8271–80.

Morris, C. and Lecar, H. (1981). Voltage oscillations in the barnacle giant muscle fiber. *Biophys J*, 35(1):193–213.

O'Keefe, J. and Burgess, N. (2005). Dual phase and rate coding in hippocampal place cells: theoretical significance and relationship to entorhinal grid cells. *Hippocampus*, 15(7): 853–66.

Pape, H. C., Paré, D., and Driesang, R. B. (1998). Two types of intrinsic oscillations in neurons of the lateral and basolateral nuclei of the amygdala. *J Neurophysiol*, 79(1):205–16.

Placantonakis, D. and Welsh, J. (2001). Two distinct oscillatory states determined by the NMDA receptor in rat inferior olive. *J Physiol*, 534(Pt 1):123–40.

Rall, W. (1967). Distinguishing theoretical synaptic potentials computed for different soma-dendritic distribution of synaptic inputs. *J Neurophysiol*, 30:1138–1168.

Remme, M. W. H., Lengyel, M., and Gutkin, B. S. (2009). The role of ongoing dendritic oscillations in single-neuron dynamics. *PLoS Comput Biol*, 5(9):e1000493.

Remme, M. W. H., Lengyel, M., and Gutkin, B. S. (2010). Democracy-independence trade-off in oscillating dendrites and its implications for grid cells. *Neuron*, 66(3):429–437.

Rinzel, J. and Ermentrout, B. (1998). *Analysis of neural excitability and oscillations. In: Koch C and Segev I, editors. Methods in neuronal modeling*, pages 251–291. MIT Press, Cambridge (MA).

Sabah, N. H. and Leibovic, K. N. (1969). Subthreshold oscillatory responses of the Hodgkin-Huxley cable model for the squid giant axon. *Biophys J*, 9(10):1206–22.

Sanhueza, M. and Bacigalupo, J. (2005). Intrinsic subthreshold oscillations of the membrane potential in pyramidal neurons of the olfactory amygdala. *Eur J Neurosci*, 22(7):1618–26.

Stuart, G., Spruston, N., and Häusser, M. (2007). *Dendrites*. Oxford University Press, New York (NY), 2nd edition.

Yoshida, M. and Alonso, A. (2007). Cell-type specific modulation of intrinsic firing properties and subthreshold membrane oscillations by the M(Kv7)-current in neurons of the entorhinal cortex. *J Neurophysiol*, 98(5):2779–94.